Communication

Facile synthesis of platinum-copper aerogels for the oxygen reduction reaction

Zhiwei Chen, Yuxiang Liao, Shengli Chen* iD

College of Chemistry and Molecular Sciences, Wuhan University, Wuhan 430072, Hubei, China.

*****Correspondence to:** Prof. Shengli Chen, College of Chemistry and Molecular Sciences, Wuhan University, Luojiashan, Wuchang District, Wuhan 430072, Hubei, China. E-mail: slchen@whu.edu.cn

Abstract

Although carbon-supported platinum (Pt/C) has been generally used as a catalyst for the oxygen reduction reaction (ORR) in fuel cells, its practical application is limited by the corrosion reaction of the carbon support. Therefore, it is essential to develop new self-supported catalysts for the ORR. Noble metal aerogels represent highly promising self-supported catalysts with large specific surface area and excellent electrocatalytic activity. Classic sol-gel processes for aerogel synthesis usually take days due to the slow gelation kinetics. Here, we report a straightforward strategy to synthesize platinum-copper (PtCu) aerogels by reducing the metal salt solution with an excess of sodium borohydride at room temperature. The PtCu aerogels are formed in a relatively short time of 1 h through a rapid nucleation mechanism. The obtained PtCu aerogels have a highly porous structure with an appreciable topological surface area of 33.0 m^2/g and mainly exposed (111) facets, which are favorable for the ORR. Consequently, the PtCu aerogels exhibit excellent ORR activity with a mass activity of 369.4 mA/mg$_{Pt}$ and a specific activity of 0.847 mA/cm^2, which are 2.6 and 3.3 times greater than those of Pt/C, respectively. The PtCu aerogels show remarkable ORR catalysis among all the noble metal aerogels that have been reported. The porous morphology and outstanding electrocatalytic activities of the PtCu aerogels illustrate their promising applications in fuel cells.

Keywords: Noble metal aerogels, platinum-copper alloy, rapid nucleation, electrocatalysis, oxygen reduction reaction

INTRODUCTION

Noble metals, especially Pt, are well known to be excellent oxygen reduction reaction (ORR) catalysts for fuel cells. However, Pt reserves are so limited that it is necessary to improve the specific mass activity of Pt. The universal ORR volcano curve indicates that decreasing the oxygen adsorption energy of Pt helps to improve its ORR catalysis performance[1] and Pt-based catalysts have been a popular research topic in recent years[2-4]. Alloying Pt with Cu is a useful strategy to reach this goal[5-8] because the strain and electron effects of Cu doping help to modify Pt[9,10]. For traditional Pt catalysts, porous carbon is used as a carrier to improve the surface area and conductivity of the catalysts. However, the carbon corrosion reaction of the carrier makes it challenging to apply Pt catalysts in practical fuel cells[11]. The construction of noble metals and their alloys as aerogels not only helps in avoiding the carbon corrosion reaction in fuel cells but also enlarges the specific surface areas and increases the porosity of the materials. Consequently, this approach improves the mass and electron transfer and thus enhances the electrocatalytic activities.

Noble metal aerogels (NMAs) originated from Eychmüller's group in 2009[12]. They proposed a two-step sol-gel process to fabricate non-supported macroscopic aerogels. During early development, the route was not satisfactory because gelation took a long period of 1-4 weeks[12]. In recent years, researchers have developed the gelation process with a number of strategies, including cation[13] and salt-inducing effects[14-21] and the use of external factors, like heating[22] and stirring[23], thereby shortening the time significantly to several hours. For higher efficiency, one-step methods have also been proposed, where the reduction and gelation take place in one pot without any other stabilizer or initiator[22-35]. The enhanced kinetics of these methods benefit the fabrication of aerogels. Among the many known aerogels, there are only a few with ORR catalytic activity, thereby inspiring us to develop appropriate catalysts for the ORR.

In this work, we demonstrate a facile one-step method for preparing Pt-based aerogels and develop PtCu aerogels with excellent electrochemical catalysis toward the ORR. Sodium chloroplatinate (Na_2PtCl_4) and copper chloride ($CuCl_2$) are reduced by $NaBH_4$, which acts not only as a reductant but also as a stabilizer and initiator, at room temperature. The PtCu aerogels are formed in tens of minutes and can be obtained after standing for several hours. The as-prepared PtCu aerogels exhibit a hierarchically porous structure with a high specific area of 33.0 m^2/g, and an outstanding ORR activity with a mass activity of 369.4 mA/mg_{Pt} and a specific activity of 0.847 mA/cm^2, which were 2.6 and 3.3 times greater than those of commercial Pt/C, respectively. The PtCu aerogels in this work are among the best Pt-based aerogel ORR catalysts that have been reported.

EXPERIMENTAL

Chemicals

Sodium chloroplatinate (Na_2PtCl_4) was provided by Sino-Platinum Metals Co., Ltd. Copper chloride dihydrate ($CuCl_2 \cdot 2H_2O$), trisodium citrate dihydrate ($C_6H_5Na_3O_7 \cdot 2H_2O$), anhydrous ethanol and methanol were purchased from Sinopharm Chemical Reagent Co., Ltd. All materials were of analytical reagent grade and used as received. Ultrapure water (18.25 mΩ·cm) from an ULUPURE UPH-III-10 water purifier was used throughout the experiments.

Synthesis of PtCu aerogels

In a typical synthesis of the PtCu aerogels, Na_2PtCl_4 (685 μL, 5×10^{-5} mol) and $CuCl_2$ (200 μL, 5×10^{-5} mol) were dissolved in ultrapure water in a 50 mL centrifuge tube to obtain an aqueous solution of 20 mL. Following that, a fresh $NaBH_4$ (5 mL, 2×10^{-3} mol) aqueous solution was shaken for several seconds and added to the tube at room temperature. The formation process of the PtCu aerogels is shown in Figure 1. In the first few minutes, a single black foam quickly formed and floated on the solution [Figure 1C]. In 1 h, the
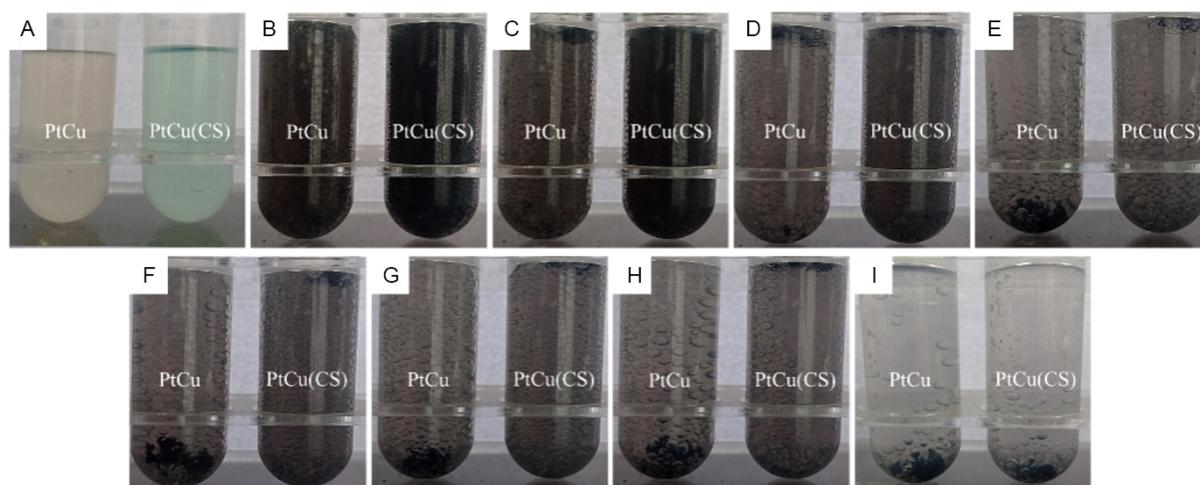
Figure 1. Digital photographs of PtCu and PtCu(CS) aerogel formation at different stages (A) before and (B) 5 min, (C) 10 min, (D) 20 min, (E) 30 min, (F) 40 min, (G) 50 min, (H) 1 h and (I) 5 h after the addition of NaBH$_4$.

aerogel was almost totally formed. The resulting mixture was settled still for another 4 h and finally sank to the bottom of the tube [Figure 1H]. The products were collected by centrifugation. The products were then washed with ultrapure water twice, ethanol/methanol (1:3) four times and ultrapure water twice. The washed products were frozen and freeze-dried in a vacuum for 12 h using a LGJ-10 freeze dryer. Finally, the PtCu aerogels were obtained.

To investigate the forming process of the PtCu aerogels, a control group was conducted. The synthesis of the control group followed a similar route but with citrate as a stabilizer in the primary step. As a result, the formation of the aerogel was slower than that without citrate [Figure 1E]. The resulting products were designated as citrate-stable platinum-copper [PtCu(CS)] aerogels.

Characterization of structure and composition
X-ray diffraction (XRD) measurements were carried out using a Rigaku Miniflex600 powder diffractometer equipped with Cu-Kα radiation, with the tube operated at a 40 kV accelerating voltage and a 15 mA current. Scanning electron microscopy (SEM) and transmission electron microscopy (TEM) images were obtained using Zeiss Merlin Compact and JEOL JEM-2100 microscopes, respectively. The samples were ground into powders for the XRD and SEM analysis. The samples were dispersed in ethanol, dropped on the ultrathin copper film and dried for the TEM analysis.

The topological surface area of the PtCu aerogels was investigated using nitrogen adsorption and desorption isotherms collected on a Micromeritics ASAP 2460 system. The chemical composition of the PtCu aerogels was confirmed by inductively coupled plasma-atomic emission spectroscopy (ICP-AES) using an IRIS Intrepid II XSP spectrometer. The samples for ICP-AES were prepared by dissolving them with aqua regia, followed by dilution.

Electrochemical measurements
Electrochemical measurements were conducted in a typical three-electrode cell using a CHI630E electrochemical workstation. Platinum foil was used as the counter electrode and a reversible hydrogen electrode (RHE) acted as the reference. The working electrode was a glassy carbon electrode (GCE) of 5 mm in diameter (Tianjin Aidahengsheng) coated with a uniform thin-film catalyst. The preparation of the

working electrode was as follows. Firstly, a certain amount of PtCu and twice as much carbon (XC-72) were mixed and dispersed in a 0.05 wt.% Nafion solution of isopropanol/water (7:3) by 1 h of ultrasonication to obtain a catalyst ink of 2.5 mg_{cat}/mL. Then, 6 μL of catalyst ink were drop-casted onto the freshly polished GCE, followed by drying at ambient temperature. Finally, a working electrode was obtained and 15 μg of catalysts were coated onto the GCE (~150 $μg_{cat}$/cm^2_{GCE}), followed by measurements of the ORR polarization and cyclic voltammetry (CV) curves. For reference, 20 wt.% commercial Pt/C was made into an ink following a similar route as above and 6 μg of Pt were coated onto GCE. All measurements were carried out in a 0.1 M $HClO_4$ aqueous solution at 30 ℃ in a water bath. ORR polarization curves were measured in an O_2-saturated solution at a rotation rate of 1600 rpm with a sweep rate of 5 mV/s between 0.1 and 1.06 V *vs.* RHE. CV curves were measured in an Ar-saturated solution with a sweep rate of 50 mV/s between 0.05 and 1.15 V *vs.* RHE.

The electrochemically active surface area (ECSA, cm^2) was obtained according to:

$$ECSA = \int JdE / v_{sweep} / \rho \tag{1}$$

Where $\int JdE$ is the integral of the absorption/desorption peak (A·V), v_{sweep} is the sweep rate of the cyclic voltammetry (V/s) and ρ is the charge density of the adsorbed/desorbed atom or molecule (C/cm^2). In this work, the hydrogen desorption region of the CV curve was chosen to calculate the ECSA and the value of ρ_H was 210 $μC/cm^2$.

The mass activities (MA, mA/mg_M) and specific activities (SA, mA/cm^2) are obtained according to equations (2) and (3), respectively:

$$MA = j_k / m_M \tag{2}$$

$$SA = j_k / ECSA \tag{3}$$

where j_k is the kinetic current (mA), which can be obtained according to the Koutecky–Levich equation:

$$1/j = 1/j_k + 1/j_d \tag{4}$$

where j is the actual current (mA) obtained from a point on the polarization curve and j_d is the limiting diffusion current (mA) obtained from the maximum current of the polarization curves. In this work, the j at 0.90 V was chosen to calculate the MA and SA.

CO-stripping voltammetry was carried out to determine the ECSA of the PtCu aerogels more delicately. The ECSA was calculated using the CO stripping peak with a ρ_{CO} of 420 $μC/cm^2$ according to equation (1). Pure PtCu was made into ink of 0.5 mg_{cat}/mL following a similar route as above. To cover all the surface, 40 μL of catalyst ink was drop-casted onto the freshly polished GCE. The route of CO-stripping started with 20 min of Ar purging to remove O_2 from the electrolyte. CO adsorption was then operated by holding the electrode at 0.1 V *vs.* RHE for 20 min with CO purging, followed by another 20 min of Ar purging to remove CO from the electrolyte. The CO-stripping peaks were measured via CV in an Ar-saturated solution with a sweep rate of 20 mV/s between 0.0 and 1.2 V *vs.* RHE.

RESULTS AND DISCUSSION

Structure and composition of PtCu aerogels

The morphology of the products was investigated by SEM and TEM. As shown in Figure 2A and B, the PtCu aerogels are sponge-like and exhibit an open hierarchical porous structure. The TEM image [Figure 2C] reveals that the PtCu aerogels were constructed of nanospheres of ~2 nm in diameter, displaying a homogeneously porous structure. The TEM image at higher magnification [Figure 2D] shows that the average spacing of the lattice fringe was measured to be 0.218 nm, which can be assigned to the (111) facet of the face-centered cubic (FCC)-structured PtCu nanoparticles. Moreover, it displayed a high crystallinity of PtCu.

The elemental distribution of the PtCu aerogels was investigated using high-angle annular dark-field scanning transmission electron microscopy (HAADF-STEM) and energy-dispersive X-ray spectroscopy (EDX). As shown in Figure 2E, both the Pt and Cu elements were evenly distributed in the PtCu aerogel framework, indicating that the structural unit nanospheres consisted of a bimetallic PtCu alloy. The XRD pattern [Figure 2F] shows that the as-prepared PtCu was quite similar to the standard FCC-structured PtCu crystal [obtained from the Joint Committee on Powder Diffraction Standards (JCPDS) File No. 48-1549]. The crystalline properties revealed by XRD agree with the TEM and HAADF-STEM-EDX analysis.

As a result, we detected the formation of PtCu aerogels following the steps below (as shown in Figure 3). At the primary stage of the reaction, both $PtCl_4^{2-}$ and Cu^{2+} were rapidly reduced by the strong reductant $NaBH_4$ together and numerous crystal nuclei of the PtCu alloy formed. The nucleus then grew into nanospheres and BH_4^- was decomposed into H_2. The violent reaction destabilized the hydrogel and accelerated the attachment of the nanospheres. Finally, the nanospheres were fused into a network and the aerogels formed in a very short time.

With the addition of citrate, the PtCu similarly grew into a sponge-like hierarchical porous structure [Figure 4A and B] and the average spacing of the lattice fringe was measured to be 0.218 nm [Figure 4D]. However, the nanospheres grew into a larger size of ~20 nm in diameter [Figure 4C] with lower crystallinity, indicating that the fusion was hindered by the coordination of citrate. This phenomenon further authenticated that the gelation of PtCu followed the rapid nucleation mechanism.

The topological surface area of the PtCu aerogels was measured to be 33.0 m²/g by the Brunauer-Emmett-Teller (BET) method. The nitrogen adsorption-desorption isotherms of the PtCu aerogels are shown in Figure 5.

Measured by ICP-AES, the exact composition of the PtCu aerogels was $Pt_{45}Cu_{55}$, in good accordance with their feed ratios.

Electrocatalytic properties of PtCu aerogels

The electrochemical catalysis of the products was investigated using the rotating disk electrode technique via a classic three-electrode system in 0.1 M $HClO_4$. Commercial 20 wt.% Pt/C catalysts were also evaluated as references. Figure 6A shows the CV curves of all these catalysts measured in an Ar-saturated 0.1 M $HClO_4$ solution at 30 ℃ with a sweep rate of 50 mV/s. According to equation (1), the ECSA values for the PtCu aerogels/C and Pt/C were determined to be 43.6 and 54.3 m²/g, respectively. CO stripping voltammetry [Figure 6D] was used to investigate the ECSA of the catalyst more delicately and was recorded in an Ar-saturated 0.1 M $HClO_4$ solution at 30 ℃ with a sweep rate of 20 mV/s. According to equation (1), the ECSA value for PtCu was determined to be 26.8 m²/g. The single peak in CO stripping curves indicated that the PtCu exposed mainly one kind of facet, in good accordance with the TEM measurement.
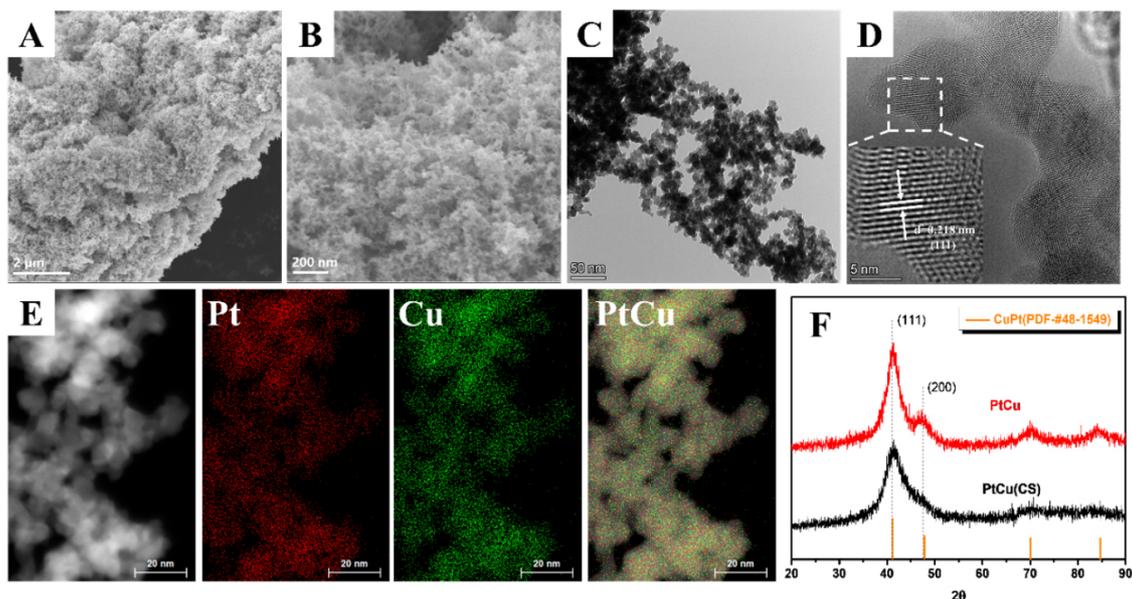
Figure 2. Structural characterization of PtCu aerogels. (A,B) SEM, (C) TEM, (D) HRTEM, (E) HAADF-STEM and EDX mapping images and (F) XRD pattern.
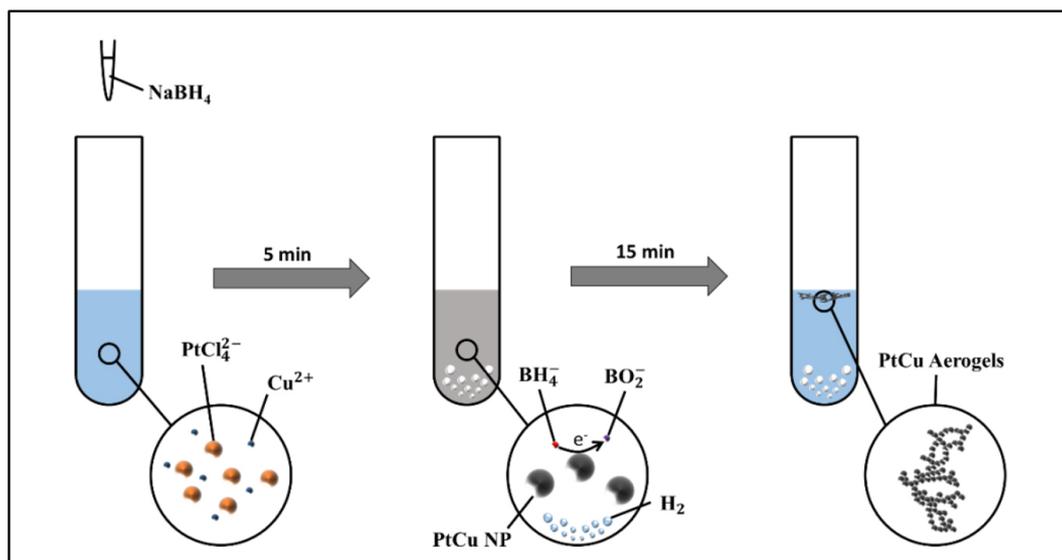

Figure 3. Schematic of PtCu aerogel formation.

The ECSA of the PtCu aerogels (26.8 m²/g) obtained from the CO-stripping curve, the topological surface area measured from the BET method (33.0 m²/g) and the ECSA of the PtCu aerogels/C (43.6 m²/g) obtained from the CV curve were quite different. The biases were attributed to the differences among the testing methods and the topological surface area was considered as the most exact one. Since a polar metal is incompatible with a non-polar GCE, the catalysts were agglomerated during the ink drying. Consequently, the catalysts have not covered the whole surface of the GCE and the apparent ECSA was smaller than the topological surface area. However, when the PtCu aerogels were mixed with carbon, the catalyst was
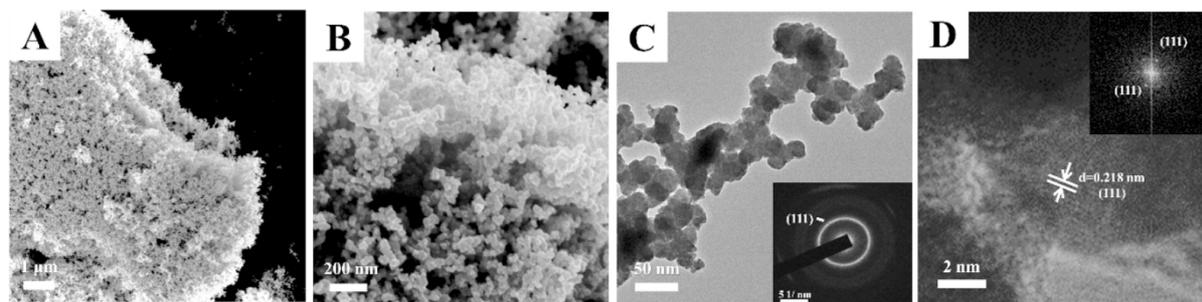
Figure 4. Structural characterization of PtCu(CS) aerogels. (A, B) SEM, (C) TEM and (D) HRTEM images. The inset in (C) is the SAED pattern recorded from (C). The inset in (D) is the corresponding FFT pattern of panel (D).
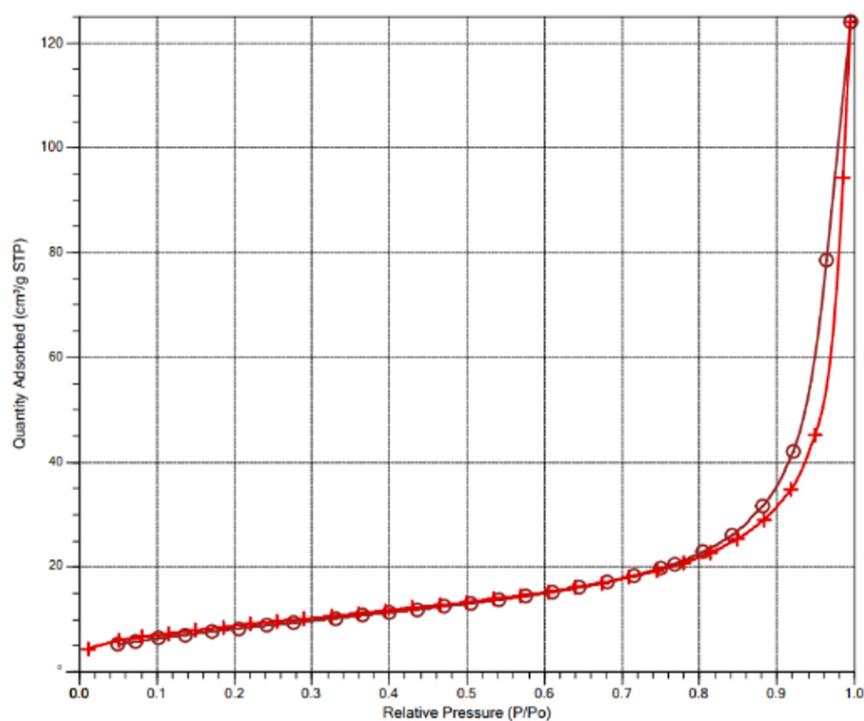

Figure 5. Nitrogen adsorption-desorption isotherms of PtCu aerogels.

dispersed into the fluffy carbon in a doping-like manner and the PtCu aerogels were effectively stretched out. Furthermore, the carbon carrier could easily cover the GCE and provide excellent conductivity. As a result, the apparent ECSA showed much higher than the topological surface area. In summary, all three kinds of surface area were credible and proved the PtCu aerogels to be porous.

The ORR polarization curves [Figure 6B] were conducted in O_2-saturated 0.1 M $HClO_4$ at 30 ℃ with a sweep rate of 5 mV/s. The ORR activities were judged by the half-wave potentials of the curves and the values for the PtCu aerogels/C and Pt/C were 0.926 and 0.888 V, respectively, indicating that the ORR catalysis of the PtCu aerogels/C is much better than that of Pt/C. The mass and specific activities of the PtCu aerogels/C and Pt/C at 0.90 V *vs.* RHE were obtained according to equations (2)-(4) and are summarized in Figure 6C. The MA values for the PtCu aerogels/C and Pt/C were 369 and 140 mA/mg$_{Pt}$, respectively. The SA values for the PtCu aerogels/C and Pt/C were 0.847 and 0.258 mA/cm^2, respectively.
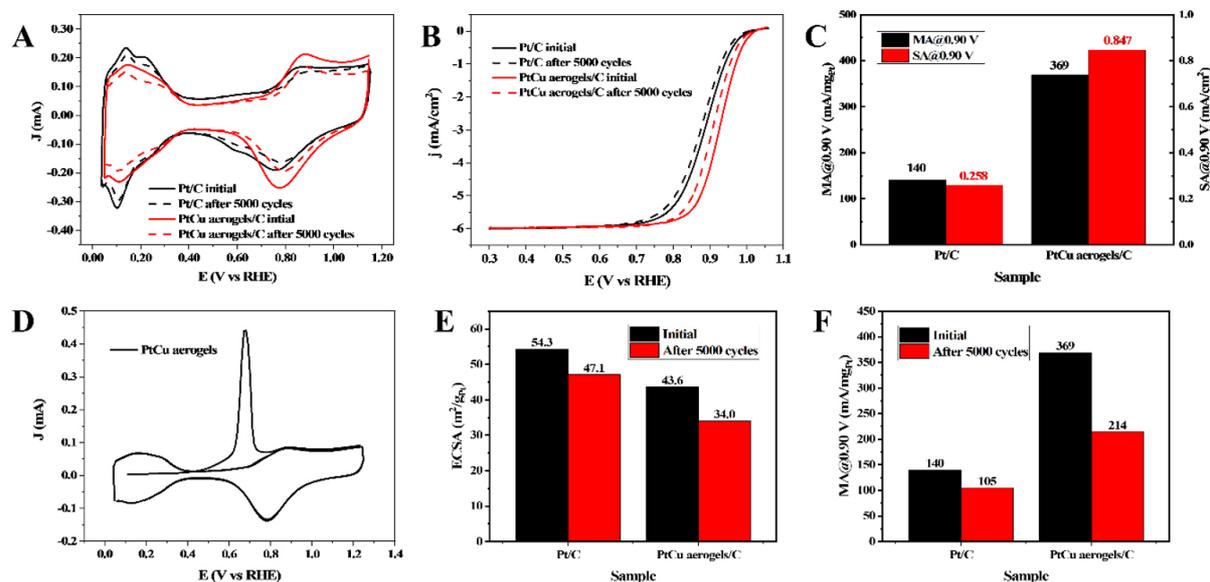
Figure 6. Electrochemical catalysis of PtCu aerogels. (A) CV curves measured at 30 ℃ in Ar-saturated 0.1 M HClO$_4$ with a sweep rate of 50 mV/s. (B) ORR polarization curves measured at 30 ℃ in O$_2$-saturated 0.1 M HClO$_4$ with a sweep rate of 5 mV/s and a rotation rate of 1600 rpm. (C) Mass and specific activities at 0.9 V *vs.* RHE. (D) CO-stripping curves measured at 30 ℃ in Ar-saturated 0.1 M HClO$_4$ with a sweep rate of 20 mV/s. (E) Mass activities at 0.9 V *vs.* RHE before and after 5000 cycles of CV. (F) ECSAs before and after 5000 cycles of CV.

Accelerated durability tests (ADTs) were conducted to investigate the stability of the PtCu aerogels/C and Pt/C by performing 5000 potential cycles in O$_2$-saturated 0.1 M HClO$_4$ at 30 ℃ with a sweep rate of 100 mV/s between 0.6 and 1.1 V *vs.* RHE. Figure 6A reveals that the CV curve of the PtCu aerogels/C was quite similar to that of Pt/C after 5000 cycles of scanning, indicating that the surfaces of PtCu were modified into the shape of Pt. Overall, the half-wave potential of the PtCu aerogels/C was reduced to 0.906 V from 0.926 V with a loss of 20 mV, and that of Pt/C was reduced to 0.877 from 0.888 V with a loss of 11 mV [Figure 6B]. The ECSA of the PtCu aerogels/C was reduced to 34.0 from 43.6 m^2/g with a loss of 22.1%, and that of Pt/C was reduced to 47.1 from 54.3 m^2/g with a loss of 13.4% [Figure 6E]. The mass activity of the PtCu aerogels/C was reduced to 214 from 369 mA/mg$_{Pt}$ with a loss of 42.2%, and that of Pt/C was reduced to 105 from 140 mA/mg$_{Pt}$ with a loss of 25.0% [Figure 6F]. Although PtCu aerogels showed less endurable than commercial Pt/C during the ADT, PtCu retained a much higher mass activity than initial commercial Pt/C.

After the ADTs, the PtCu aerogels/C were transferred into an ethanol solvent from the GCE by ultrasonication and then investigated by HAADF-STEM and EDX mapping. As shown in Figure 7A, the PtCu aerogels maintained the three-dimensional structure. However, it also revealed an obvious agglomeration phenomenon, which explained the performance degradation during the ADT. Figure 7B reveals that the average spacing of lattice fringe was measured to be 0.218 nm, indicating that the PtCu alloy could maintain its crystal structure. EDX mapping [Figure 7C] revealed that the atom fractions of Pt and Cu were 53.9% and 46.1%, respectively, indicating that the elemental distribution almost never changed during the potential cycles. The credible stability of the crystal structure and elemental distribution may explain the high mass activity investigated after the ADT.

A comparison of the electrochemical catalysis for both the PtCu aerogels/C and Pt/C investigated before and after ADT is summarized in Table 1. The MA and SA of the PtCu aerogels were 2.6 and 3.3 times greater than those of commercial Pt/C, respectively. Furthermore, the PtCu aerogels maintained high MA after 5000 potential cycles.

Table 1. Comparison of electrochemical catalysis

Samples	ECSA (m²/g)			MA (mA/mg$_{Pt}$)			Half-wave potential (V)		
	Initial	After ADT	Loss	Initial	After ADT	Loss	Initial	After ADT	Loss
PtCu aerogels/C	43.6	34.0	22.1%	369.4	213.7	42.3%	0.926	0.906	0.020
Pt/C	54.3	47.1	13.4%	140.0	105.0	25.0%	0.885	0.873	0.012
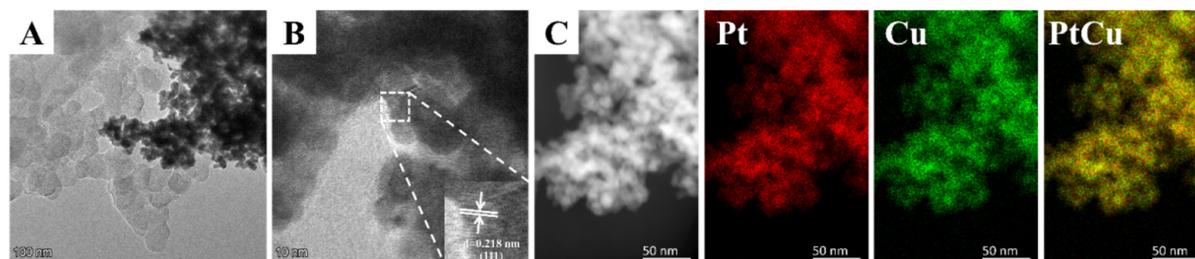
Figure 7. Structural characterization of PtCu aerogels/C obtained after ADT. (A, B) HRTEM images and (C) HAADF-STEM and EDX mapping images.

We considered that the enhanced ORR activity of the PtCu aerogels may originate from two aspects. For the topological structure of the PtCu aerogels, the high specific area provided more active sites and the larger porosity helped improve the mass transfer. For the crystal structure of the PtCu alloy, alloying with Cu lowers the d-band center of Pt and consequently weakens the oxygen adsorption energy of Pt, helping increase the activity[1]. Furthermore, the PtCu exposed mainly (111) facets, which is the best facet for catalyzing ORR[36]. As a result, the PtCu aerogels exhibited excellent electrochemical catalysis towards the ORR.

CONCLUSIONS

In conclusion, PtCu aerogels were successfully synthesized by a facile NaBH$_4$ reduction reaction and showed a porous structure with high specific surface areas. The synthesis period was effectively reduced from tens of hours to tens of minutes. By controlling the addition of citrate, we discussed that the gelation of PtCu followed the rapid nucleation mechanism. Moreover, the as-prepared PtCu aerogels exposed mainly the most active facets for the ORR and consequently exhibited a remarkable ORR performance compared to Pt/C. This facile route and good catalytic activity may help develop efficient catalysts for fuel cell applications.

DECLARATIONS

Authors' contributions
Experiments, data analysis and manuscript writing: Chen Z
Assistance in experiments and data analysis: Liao Y
Supervision of the research: Chen S

Availability of data and materials
Not applicable.

Conflicts of interest

All authors declared that there are no conflicts of interest.

Ethical approval and consent to participate

Not applicable.

Consent for publication

Not applicable.

REFERENCES

1. Nørskov JK, Rossmeisl J, Logadottir A, et al. Origin of the overpotential for oxygen reduction at a fuel-cell cathode. *J Phys Chem B* 2004;108:17886-92. DOI
2. Yu Y, Xia F, Wang C, et al. High-entropy alloy nanoparticles as a promising electrocatalyst to enhance activity and durability for oxygen reduction. *Nano Res* 2022;15:7868-76. DOI
3. Lu R, Quan C, Zhang C, et al. Establishing a theoretical insight for penta-coordinated iron-nitrogen-carbon catalysts toward oxygen reaction. *Nano Res* 2022;15:6067-75. DOI
4. Jang I, Lee S, Jang J, Ahn M, Yoo SJ. Improved platinum-nickel nanoparticles with dopamine-derived carbon shells for proton exchange membrane fuel cells. *Intl J of Energy Res* 2022;46:13602-12. DOI
5. Sohn Y, Park JH, Kim P, Joo JB. Dealloyed PtCu catalyst as an efficient electrocatalyst in oxygen reduction reaction. *Curr Appl Phys* 2015;15:993-9. DOI
6. Wu D, Yang Y, Dai C, Cheng D. Enhanced oxygen reduction activity of PtCu nanoparticles by morphology tuning and transition-metal doping. *Int J Hydrog Energy* 2020;45:4427-34. DOI
7. Garcia-cardona J, Sirés I, Alcaide F, Brillas E, Centellas F, Cabot PL. Electrochemical performance of carbon-supported Pt(Cu) electrocatalysts for low-temperature fuel cells. *Int J Hydrog Energy* 2020;45:20582-93. DOI
8. Pavlets A, Alekseenko A, Tabachkova NY, et al. A novel strategy for the synthesis of Pt–Cu uneven nanoparticles as an efficient electrocatalyst toward oxygen reduction. *Int J Hydrog Energy* 2021;46:5355-68. DOI
9. Strasser P, Koh S, Anniyev T, et al. Lattice-strain control of the activity in dealloyed core-shell fuel cell catalysts. *Nat Chem* 2010;2:454-60. DOI PubMed
10. Stephens IE, Bondarenko AS, Perez-Alonso FJ, et al. Tuning the activity of Pt(111) for oxygen electroreduction by subsurface alloying. *J Am Chem Soc* 2011;133:5485-91. DOI PubMed
11. Zhao J, Tu Z, Chan SH. Carbon corrosion mechanism and mitigation strategies in a proton exchange membrane fuel cell (PEMFC): a review. *J Power Sources* 2021;488:229434. DOI
12. Bigall NC, Herrmann AK, Vogel M, et al. Hydrogels and aerogels from noble metal nanoparticles. *Angew Chem Int Ed Engl* 2009;48:9731-4. DOI PubMed
13. Wen D, Herrmann AK, Borchardt L, et al. Controlling the growth of palladium aerogels with high-performance toward bioelectrocatalytic oxidation of glucose. *J Am Chem Soc* 2014;136:2727-30. DOI PubMed
14. Du R, Hu Y, Hübner R, et al. Specific ion effects directed noble metal aerogels: versatile manipulation for electrocatalysis and beyond. *Sci Adv* 2019;5:eaaw4590. DOI PubMed PMC
15. Ranmohotti KGS, Gao X, Arachchige IU. Salt-mediated self-assembly of metal nanoshells into monolithic aerogel frameworks. *Chem Mater* 2013;25:3528-34. DOI
16. Gao X, Esteves RJ, Luong TT, Jaini R, Arachchige IU. Oxidation-induced self-assembly of Ag nanoshells into transparent and opaque Ag hydrogels and aerogels. *J Am Chem Soc* 2014;136:7993-8002. DOI PubMed
17. Gao X, Esteves RJ, Nahar L, Nowaczyk J, Arachchige IU. Direct cross-linking of Au/Ag Alloy nanoparticles into monolithic aerogels for application in surface-enhanced raman scattering. *ACS Appl Mater Interfaces* 2016;8:13076-85. DOI PubMed
18. Nahar L, Farghaly AA, Esteves RJA, Arachchige IU. Shape controlled synthesis of Au/Ag/Pd nanoalloys and their oxidation-induced self-assembly into electrocatalytically active aerogel monoliths. *Chem Mater* 2017;29:7704-15. DOI
19. Naskar S, Freytag A, Deutsch J, et al. Porous aerogels from shape-controlled metal nanoparticles directly from nonpolar colloidal solution. *Chem Mater* 2017;29:9208-17. DOI
20. Wen D, Liu W, Haubold D, et al. Gold aerogels: three-dimensional assembly of nanoparticles and their use as electrocatalytic interfaces. *ACS Nano* 2016;10:2559-67. DOI PubMed PMC

21.   Wen D, Liu W, Herrmann AK, et al. Simple and sensitive colorimetric detection of dopamine based on assembly of cyclodextrin-modified Au nanoparticles. *Small* 2016;12:2439-42. DOI PubMed

22.   Zhu C, Shi Q, Fu S, et al. Efficient synthesis of MCu (M = Pd, Pt, and Au) aerogels with accelerated gelation kinetics and their high electrocatalytic activity. *Adv Mater* 2016;28:8779-83. DOI PubMed

23.   Du R, Joswig JO, Fan X, et al. Disturbance-promoted unconventional and rapid fabrication of self-healable noble metal gels for (photo-)electrocatalysis. *Matter* 2020;2:908-20. DOI PubMed PMC

24.   Liu W, Herrmann AK, Geiger D, et al. High-performance electrocatalysis on palladium aerogels. *Angew Chem Int Ed Engl* 2012;51:5743-7. DOI PubMed

25.   Henning S, Ishikawa H, Kühn L, et al. Unsupported Pt-Ni aerogels with enhanced high current performance and durability in fuel cell cathodes. *Angew Chem Int Ed Engl* 2017;56:10707-10. DOI PubMed

26.   Liu W, Rodriguez P, Borchardt L, et al. Bimetallic aerogels: high-performance electrocatalysts for the oxygen reduction reaction. *Angew Chem Int Ed Engl* 2013;52:9849-52. DOI PubMed

27.   Shi Q, Zhu C, Du D, et al. Kinetically controlled synthesis of AuPt bi-metallic aerogels and their enhanced electrocatalytic performances. *J Mater Chem A* 2017;5:19626-31. DOI

28.   Shi Q, Zhu C, Zhong H, et al. Nanovoid incorporated Ir x Cu metallic aerogels for oxygen evolution reaction catalysis. *ACS Energy Lett* 2018;3:2038-44. DOI

29.   Wang H, Wu Y, Luo X, et al. Ternary PtRuCu aerogels for enhanced methanol electrooxidation. *Nanoscale* 2019;11:10575-80. DOI PubMed

30.   Shi Q, Zhu C, Tian M, et al. Ultrafine Pd ensembles anchored-Au$_2$Cu aerogels boost ethanol electrooxidation. *Nano Energy* 2018;53:206-12. DOI

31.   Zhu C, Shi Q, Fu S, et al. Core-shell PdPb@Pd aerogels with multiply-twinned intermetallic nanostructures: facile synthesis with accelerated gelation kinetics and their enhanced electrocatalytic properties. *J Mater Chem A* 2018;6:7517-21. DOI

32.   Burpo FJ, Nagelli EA, Morris LA, Mcclure JP, Ryu MY, Palmer JL. Direct solution-based reduction synthesis of Au, Pd, and Pt aerogels. *J Mater Res* 2017;32:4153-65. DOI PubMed PMC

33.   Yazdan-abad M, Noroozifar M, Modaresi Alam AR, Saravani H. Palladium aerogel as a high-performance electrocatalyst for ethanol electro-oxidation in alkaline media. *J Mater Chem A* 2017;5:10244-9. DOI

34.   Yazdan-abad M, Noroozifar M, Douk AS, Modarresi-alam AR, Saravani H. Shape engineering of palladium aerogels assembled by nanosheets to achieve a high performance electrocatalyst. *Appl Catal B* 2019;250:242-9. DOI

35.   Douk A, Saravani H, Noroozifar M. Three-dimensional assembly of building blocks for the fabrication of Pd aerogel as a high performance electrocatalyst toward ethanol oxidation. *Electrochim Acta* 2018;275:182-91. DOI

36.   Kondo S, Nakamura M, Maki N, Hoshi N. Active sites for the oxygen reduction reaction on the low and high index planes of palladium. *J Phys Chem C* 2009;113:12625-8. DOI